



Tensegrity topology optimization by force maximization on arbitrary ground structures

Ke Liu¹ · Glaucio H. Paulino¹

Received: 13 February 2017 / Revised: 27 November 2018 / Accepted: 29 November 2018 / Published online: 31 January 2019
© Springer-Verlag GmbH Germany, part of Springer Nature 2019

Abstract

This paper presents an optimization approach for design of tensegrity structures based on graph theory. The formulation obtains tensegrities from ground structures, through force maximization using mixed integer linear programming. The method seeks a topology of the tensegrity that is within a given geometry, which provides insight into the tensegrity design from a geometric point of view. Although not explicitly enforced, the tensegrities obtained using this approach tend to be both stable and symmetric. Borrowing ideas from computer graphics, we allow “restriction zones” (i.e., passive regions in which no geometric entity should intersect) to be specified in the underlying ground structure. Such feature allows the design of tensegrities for actual engineering applications, such as robotics, in which the volume of the payload needs to be protected. To demonstrate the effectiveness of our proposed design method, we show that it is effective at extracting both well-known tensegrities and new tensegrities from the ground structure network, some of which are prototyped with the aid of additive manufacturing.

Keywords Tensegrity · Form-finding · Ground structure · Topology optimization · Graph theory · Additive manufacturing

1 Introduction

Snelson (2012) referred to tensegrity as the art of “floating compression structures.” According to Fuller (1962), the word tensegrity is a contraction of the words “tensile” and “integrity,” which refers to a continuous network of tension. However, historically, tensegrity has not been given a unique technical definition (Motro 2006; Skelton and de Oliveira 2009). Although the tensegrity concept is ubiquitous, the actual word is interpreted differently across fields, such as architecture, engineering, art, mathematics, and biology.

In the most general definition, the term “tensegrity” encompasses any prestressed structural system that has continuous tensile component, like membranes. For example, in

biology, Ingber (1998) interpreted tensegrity as the fundamental structure of all living creatures with the distinctive characteristic of being prestressed and having a continuous tensile component, such as the cytoskeleton of cells. Classic tensegrities like the sculptures by Heartney and Snelson (2009), align with the definition by Motro (2006): “A tensegrity system is a system in a stable self-equilibrated state comprising a discontinuous set of compressed components inside a continuum of tensioned components.” Other definitions can also be found (see Connelly and Whiteley 1996). Some might insist that a tensegrity must also have infinitesimal mechanisms. However, in this work, kinematic indeterminacy is not a particular feature of interest (see last paragraph of Section 3.1). The structures that we design follow the definitions by researchers such as Motro (2006), Zhang and Ohsaki (2015), and Skelton and de Oliveira (2009). Since we only consider rectilinear members, our designed structures can also be called “strut-tendon” structures, as introduced by Hanaor (2012). In addition, we adopt the classification of tensegrity according to Skelton and de Oliveira (2009) and Williamson and Skelton (2003) in order to generalize the concept of tensegrity by relaxing the discontinuity constraint regarding struts. The Class definition sets an upper bound to the number of compressive members (i.e., struts) that can connect at each node of the tensegrity.

Responsible Editor: Anton Evgrafov

Dedicated to the memory of Mr. Kenneth Snelson (1927–2016).

✉ Glaucio H. Paulino
paulino@gatech.edu

Ke Liu
ke.liu@gatech.edu

¹ School of Civil and Environmental Engineering, Georgia Institute of Technology, Atlanta, GA 30332, USA

For example, the iconic “Needle Tower” shown in Fig. 1a is a Class-1 tensegrity, for which the struts are all isolated. As an example of a Class-2 tensegrity, we cite the work by Moored et al. (2011), who designed an active robotic fin for underwater locomotion. For further details about the history and definitions of tensegrity, the readers are referred to the book by Motro (2006).

Tensegrity has shown significant potential for engineering applications (Schenk et al. 2007). The idea has been used to make structures that are deployable, actively tunable, and light weight (Caluwaerts et al. 2014; Motro 2006; Schenk et al. 2007; Sultan 1999; Tibert 2002; Rhode-Barbarigos 2012; Hanaor and Liao 1991; Pellegrino 1992; Liu et al. 2017). Moreover, tensegrity properties have also been explored to design novel lattice materials that could reach superior strength-to-weight ratio (Rimoli and Pal 2016). Because design of new tensegrities for specific applications is challenging, most applications rely on existing tensegrity forms. Thus, the aim of our work is to provide a method that allows the creation of tensegrity designs by means of topology optimization.

Some analytical and numerical approaches have been proposed in the literature for form-finding of tensegrity. *The design of a tensegrity has two main aspects: the topology and the geometry.* We can classify the form-finding methods into two categories: topology design methods and geometry design methods. The distinction is based on the way to achieve self-equilibrium of the structure during the design: by adjusting either the topology or the geometry. For a typical geometry design method, the topology of the tensegrity is first defined; then, the geometry evolves to achieve self-equilibrium (Li et al. 2010a; Tachi 2013; Zhang and Ohsaki 2006; Ohsaki and Zhang 2015; Lee and Lee 2016). Most numerical form-finding approaches fall into this category. On the contrary, for a topology

design method, the geometry is specified a priori, while the topology evolves to ensure self-equilibrium (Ehara and Kanno 2010; Kanno 2012, 2013a, b; Xu et al. 2016). The two categories are not mutually exclusive. A method can belong to both categories, for example, design by intuition. A detailed review of form-finding methods is presented in Section 2.

Here, we propose a numerical approach for the design of tensegrity in the category of the “topology design method.” We perform a mixed integer linear programming (MILP) on ground structures to extract the tensegrity design. The ground structure method has been used in the field of (structural) topology optimization for a long time (Dorn et al. 1964; Smith 1998; Zegard and Paulino 2015). It provides a very dense set of potential members and joints from which the desired structure can be extracted through the optimization process. In topology optimization of tensegrity, the method selects members from the ground structure and finds the associated self-equilibrating prestress forces. All joints have fixed coordinates during the optimization; thus, the geometry of the tensegrity is fixed, featuring a prescribed geometry.

The impact of this research stands out by two main concepts: the development of a new tensegrity form-finding formulation, which yields effective design of tensegrities with fixed geometry, and the extension to use arbitrary shapes as the building blocks, with the possibility of concave geometric constraints such as holes and openings. The proposed formulation is relatively simple and computationally efficient compared to similar formulations (Ehara and Kanno 2010; Kanno 2012, 2013a, b; Xu et al. 2016), and often converges to symmetric and stable structures. An overview of tensegrity form-finding methods is provided in Section 2, while the actual topology optimization formulation, rooted on graph theory,

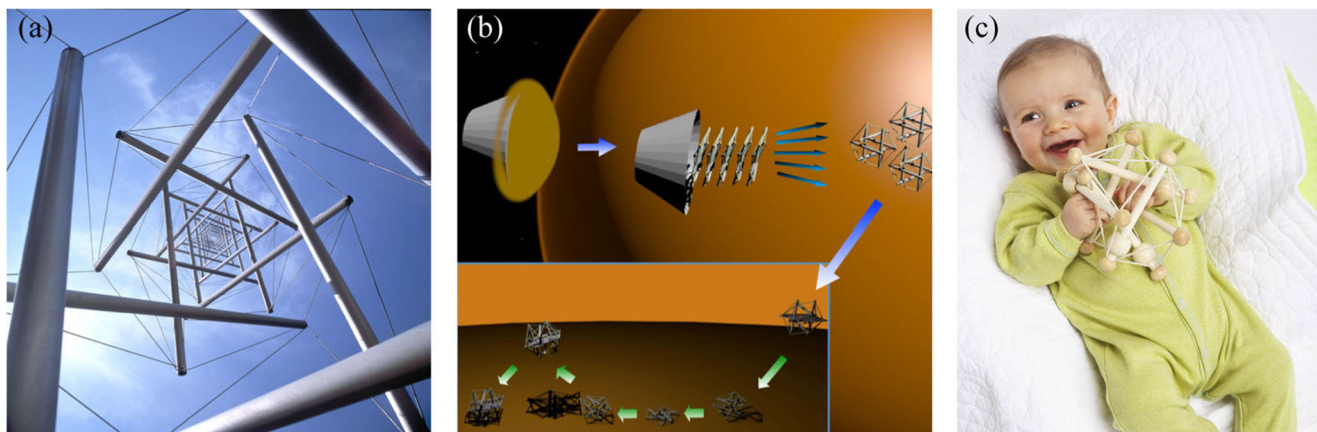


Fig. 1 Applications of tensegrity structures. **a** The outdoor sculpture “Needle Tower” created by Kenneth Snelson (1968) (Heartney and Snelson 2009) (image courtesy of Kenneth Snelson.) **b** Tensegrity robot design investigated by NASA (Caluwaerts et al. 2014) for outer

space missions (adapted from Caluwaerts et al. 2014.) **c** A baby playing with a tensegrity toy (image reproduced from Manhattan 2018. ©2018 Manhattan Toy)

is presented in detail in Section 3. Borrowing from the techniques that we have previously developed on the generation of complex three-dimensional ground structures (Zegard and Paulino 2015), we can impose different passive zones in the ground structure, which are useful for designing tensegrities aimed at actual engineering applications. For example, in the design of tensegrity for outer space exploration (Caluwaerts et al. 2014), some interior spaces need to be reserved for payloads. Combining these new features, the present formulation is able to reproduce many of the known forms of tensegrity, as verified in Section 4 and Appendix 1. With the confidence provided by the verification study, we use our method to discover and design new tensegrity structures, as shown in Sections 4 and 5. Section 6 presents a discussion of the numerical aspects of the work. Some of the designs are prototyped with physical models, using a simple procedure, aided by 3D printing technology, which is elaborated in Section 7. Four appendices complement the present work, which include reproducing known tensegrities, illustrating topological constraints by means of an example, describing basic structural analysis of tensegrities, and providing the Nomenclature adopted in the present work.

2 Overview of form-finding methods

In this section, we cast the forming-finding problem of tensegrity in a generic form and discuss how different methods fit into the framework. As a kind of prestressed discrete structure connected by joints, the configuration of a tensegrity is totally defined by the following components:

- (1) Topology, which can be described using a graph G
- (2) Geometry, which is defined by the coordinates \mathbf{p} of the nodes
- (3) Self-equilibrium state, which contains the self-equilibrating prestress forces in the members (stored in a vector \mathbf{F})

The topology of such structures can be described using a graph G , which contains a set of vertices V and edges E , where edges reflect the pairing of vertices. The vertices of the graph can be interpreted as the indexing of the nodes of a tensegrity structure, and the edges represent the members. The geometry of a tensegrity is a map that assigns each vertex in the graph with a coordinate in the Euclidean space \mathbb{R}^d of dimension d . In this paper, we restrict our scope to $d = 3$. The geometry can be represented by \mathbf{p} , a $3N_V \times 1$ vector that stores the (x, y, z) coordinates of each node sequentially. Furthermore, an associated self-equilibrium state is essential for a tensegrity structure by definition. The self-equilibrating state is sustained by a set of forces attached to each member of the structure, such that struts are in compression and cables are in tension.

The form-finding of tensegrity structures consists of finding a graph with associated geometry over the vertices and self-equilibrating forces over the edges. In general, a form-finding problem of tensegrity can be expressed as follows:

$$\text{Find: } G, \mathbf{p}, \mathbf{F} \quad (1a)$$

$$\text{such that: } \mathbf{B}(\mathbf{p}, G)\mathbf{F} = \mathbf{0} \quad (1b)$$

$$T(G) \leq n \quad (1c)$$

$$\mathbf{u}^T \mathbf{K} \mathbf{u} > 0,$$

$$\text{for any nontrivial displacement } \mathbf{u} \quad (1d)$$

The equilibrium matrix \mathbf{B} is determined by \mathbf{p} and G (see Appendix 3 for its derivation). The prestress forces \mathbf{F} should self-equilibrate the tensegrity, as stated in condition (1b). The term \mathbf{K} is the tangent stiffness matrix of the tensegrity which depends on the topology G , geometry \mathbf{p} , and prestress forces \mathbf{F} , as well as member properties such as cross-sectional areas and material properties. Condition (1c) is a topological constraint which restricts the number of compressive members that can meet at each vertex. For Class-1 tensegrity, $n = 1$, that is, the compressive members are all disconnected (i.e. floating). In order to ensure that the tensegrity structure is free-standing, we also need to examine its stability. Condition (1d) is the stability requirement stating that the quadratic form of the tangent stiffness matrix with respect to any small nontrivial displacement of nodes is positive, which, in addition to the equilibrium constraint, implies that the total potential energy of the structure at its initial state is at a strict local minimum. The infinitesimal displacement of nodes, i.e., \mathbf{u} , is trivial if it represents a rigid-body motion or if it is a zero vector. It is equivalent to say that \mathbf{K} is positive definite after constraining the rigid-body motions. Assuming the elastic structure undergoes very small deformations, the tangent stiffness matrix is composed of a linear stiffness matrix \mathbf{K}_E and a geometrical stiffness matrix \mathbf{K}_G (Guest 2006, 2011; Zhang and Ohsaki 2015). In this paper, because we assume that the strains in members are small, including prestrains (i.e., initial deformations) induced by the prestress, then it is sufficient to construct only the so-called stress matrix (Connelly 1999) as an approximation to the complete geometric stiffness matrix (Guest 2006, 2011; Schenk et al. 2007). A brief derivation is presented in Appendix 3.

The aforementioned stability condition is the minimum potential energy stability. However, the tangent stiffness matrix requires information about member properties, which can be cumbersome for preliminary studies (Zhang and Ohsaki 2015). There are two other criteria that are usually used in the study of stability of tensegrities, namely, prestress stability and super-stability. Assume the rigid-body motions are already properly restricted for a tensegrity. Prestress stability requires that the quadratic form $\mathbf{u}_M^T \mathbf{K}_G \mathbf{u}_M$ be positive, for all $\mathbf{u}_M \in \{\mathbf{u} : \mathbf{B}^T \mathbf{u} = \mathbf{0}, \mathbf{u} \neq \mathbf{0}\}$. The transpose of the equilibrium matrix is the compatibility

matrix (Guest 2006). A special case of prestress stability is when the compatibility matrix has full row rank, which indicates there is no \mathbf{u}_M , and such a tensegrity is said to be infinitesimally rigid (Connelly and Whiteley 1996). We clarify here that \mathbf{u}_M preserves the lengths of all members, however, in an actual tensegrity, the cables can be shortened (i.e., slacked). When a tensegrity is said to be kinematically determinate, it actually means that the dual truss structure (if we replace all the members in a tensegrity with bars) that has the same geometry and topology is kinematically determinate. Notice that a kinematically determinate tensegrity is not equivalent to a kinematically determinate truss. An infinitesimally rigid truss is structurally stable; however, an infinitesimally rigid tensegrity may or may not be structurally stable without prestress because of slackness of cables. As proved by Connelly and Whiteley (1996), an infinitesimally rigid tensegrity is only guaranteed to be stable with the presence of prestress. In addition to the prestress stability, if the geometrical stiffness matrix \mathbf{K}_G (or the stress matrix in the current context) is positive semi-definite with maximal rank that equals to $3N_V - d(d + 1)$ (Connelly 1999; Schenk et al. 2007), then the structure is super-stable. In general, super-stability ensures minimum potential energy stability of the structure; however, a high level of prestress can make a super-stable tensegrity unstable owing to the significant initial deformations induced by prestress (Guest 2011). Therefore, in this paper, we assume that the prestrains of members are small. Super-stability is usually preferred because prestress stability is only a necessary condition for a stable structure (Zhang and Ohsaki 2015). In many form-finding approaches, conditions (1b) and (1c) are the basic constraints, while condition (1d) may not be considered at first since it complicates the form-finding process. It is usually checked a posteriori, i.e., after the design is obtained.

The tensegrity design problem has been solved using intuition, analytical methods, and numerical methods. Analytical and intuitive methods of form-finding seek the topology and geometry simultaneously (Connelly 1995). Only a small number of known solutions have been obtained analytically or based on intuition, and application of these solutions is limited due to the small number of known configurations. Numerical form-finding methods are usually done by first fixing either the topology or the geometry, and then finding the other to achieve self-equilibrium. Geometry design methods fix the topology and search for the geometry of a tensegrity as well as the corresponding self-equilibrium state. Examples of geometry design methods are adaptive force density method (Zhang and Ohsaki 2006), free-forming method (Tachi 2013), dynamic relaxation method (Zhang et al. 2006), and Monte Carlo form-finding method (Li et al. 2010b). Because one topology can have many

geometries that are associated with a set of self-equilibrating forces, the obtained geometry always has some arbitrariness. The initial assignment of the topology is also tricky. Typically, it is based on heuristic rules evolved from planar diagrams (Li et al. 2010a; Tachi 2013). Thus, if such methods are used to generate tensegrities with many members occupying a large space, a common characteristic of the final result is that the connectivities are local and the obtained geometries become hollow (i.e. no members crossing the internal space).

Topology design methods, which fix the geometry of the tensegrity and search for the topology and the underlying self-equilibrium state, have only emerged in recent years (Ehara and Kanno 2010; Kanno 2012, 2013a, b; Xu et al. 2016). A ground structure is used to provide the candidate members for the self-equilibrating forces to attach to, and the topology of the tensegrity is determined as a consequence. A typical drawback of such methods is that, due to the discrete nature of the topology, the problem is usually difficult to solve. However, the advantage is that one does not need to prescribe the topology, which is hard to guess at an initial design stage. Ehara and Kanno (2010) proposed a two-step mixed integer linear programming (MILP) formulation, in which they first maximize the number of struts and then minimize the number of cables. Kanno (2012, 2013a, b) explored other one-step formulations with various objective functions and constraints, for example, minimization of total length of cables, minimization of compliance under some external loads, implicit symmetry constraint, kinematic indeterminacy constraint, and contact constraint. In this paper, we propose a different objective function defined solely on the continuous variables in the MILP, which implicitly promotes stability and symmetry of the optimized design.

3 Topology optimization formulation

The proposed form-finding formulation is an optimization approach based on the ground structure method. The formulation does not enforce the stability of the tensegrity, but we will see that the method is prone to converge to a stable tensegrity. The obtained designs also inherit the symmetries possessed by the initial ground structures.

3.1 Formulation

Denote G_g as the graph that represents the topology of the ground structure. Its vertices V_g and edges E_g are the sets of all nodes and members, respectively. The force vector \mathbf{F} contains the forces in members (i.e., E_g), which are the design variables. Any nonzero entry in the solution

implies the existence of a corresponding member. A force attached to member e with $F_e < 0$ is a compressive force. The proposed form-finding method takes the following mathematical form:

$$\max_{\mathbf{F}} \mathbf{1}^T \mathbf{F} \quad (2a)$$

$$\text{s.t.} \quad \mathbf{B}\mathbf{F} = \mathbf{0} \quad (2b)$$

$$\sum_{e \sim v} \chi(F_e) \leq n, \forall v \in V_g \quad (2c)$$

$$-1 \leq F_e, \forall e \in E_g \quad (2d)$$

$$\text{with:} \quad \chi(F_e) = \begin{cases} 1, & F_e < 0 \\ 0, & F_e \geq 0 \end{cases} \quad (2e)$$

The indicator function χ is a binary operator that indicates the presence of struts, as stated in (2e). The notation $e \sim v$ denotes that the edge e is incident on vertex v . In other words, member e is connected to vertex v . Thus, the second constraint in (2c) enforces the discontinuity of struts. The compressive forces are constrained with a maximal magnitude in (2d), as the null space of \mathbf{B} is unbounded. Physically, for a finite self-stressed discrete structure, the entries of a nontrivial \mathbf{F} cannot be all positive or all negative—thus, it is enough to impose only the constraint (2d) on the magnitude of compression forces to ensure that the feasible domain is bounded. Members in the ground structure that are not attached with any force are excluded from the optimized structure.

The trivial solution $\mathbf{F} = \mathbf{0}$ is always feasible and any nonzero feasible solution makes a tensegrity if neglecting the stability requirement. To find a desired solution to this under-determined system, an additional criterion is necessary. Here, we choose to maximize the sum of forces in the structure, that is, the difference between total tension and compression. Intuitively, this objective will prompt structures that span the maximal space bounded by the ground structure such that we avoid trivial solutions. Based on observation, the objective function seems to favor a larger number of struts. A heuristic explanation is given as follows. To maintain equilibrium, when the total compression in the structure increases, the total tension should increase accordingly, but usually at a faster rate (based on observation). Therefore, the difference between the sum of absolute tension and the sum of absolute compression, which is our objective function, tends to increase as the total compression increases. As the compressive force in each member is bounded, a larger number of compressive members are favored, possibly providing a higher sum of the compressive forces.

In addition to avoiding trivial solutions, the proposed objective leads to tensegrities with two other desirable properties. First, the objective tends to generate tensegrity structures that are stiff and stable. Note that as the difference between total tension and total compression is maximized,

the ratio of total compression to total tension is minimized. This ratio can be regarded as a measure for the average angle between struts and cables, as illustrated in Fig. 2. When the ratio of total compression to total tension is smaller, the average angle between struts and cables is larger (i.e., closer to orthogonal). From a structural engineering point of view, each strut is provided with more efficient bracing by the cables that will help to stabilize the prestressed structures. An example from daily life is the bicycle wheel, in which the compressive forces are almost orthogonal to tensile forces.

Furthermore, the formulation encourages convergence to a structure that preserves some symmetries of the prescribed ground structure. Suppose that we have a symmetric ground structure G_g associated with a non-degeneratable symmetry group H that contains some transformations $h_i \in H$. Each transformation h_i of nodes and members of the ground structure is a symmetry operation under which the structure is unchanged (Guest 2000; Zhang et al. 2009; Zhang and Ohsaki 2015).

Because this problem is a discrete programming problem, which is complicated, we first look at a relaxed version of formulation (3.1) to check the symmetry preserving property of the optimal solution to this force maximization problem. Note that by increasing the integer n in constraint (2c), the topological constraint becomes inactive and we achieve a linear programming (LP) problem. We first show that when the topological constraint is inactive, the optimal solution of the resultant LP problem could preserve all symmetries of the initial ground structure. Let \mathbf{F} be a feasible solution of the LP problem that satisfies all the constraints. Since the objective function pushes more tension than compression, we can consider only \mathbf{F} 's with $\mathbf{1}^T \mathbf{F} \geq 0$. If $\mathbf{1}^T \mathbf{F} \leq 0$, we can simply multiply \mathbf{F} by a factor of -1 . Let G represent the topology of the structure indicated by \mathbf{F} . There exists a scalar $\xi \geq 1$, such that:

$$\min(\xi \mathbf{F}) = \min_i(\xi F_i) = -1. \quad (3)$$

Clearly, $\xi \mathbf{F}$ is a feasible solution, and it yields maximal objective on topology G along direction \mathbf{F} . Associated with G , suppose there is a non-degenerate symmetry group K that is a subgroup of H , with symmetry operations $k_i \in K$, such that $k_i(G) = G$. If K is not equal to H , we can construct a new solution:

$$\mathbf{F}' = \mathbf{F}/(m+1) + \sum_{j=1}^m h_j(\mathbf{F})/(m+1), \text{ with } h_j \in H, h_j \notin K. \quad (4)$$

The number m counts the number of symmetry operations h_j as defined in (4). By applying a transformation $h_j (\notin K)$ to G , we obtain a structure represented by $h_j(G)$, which is a different subset of G_g , as demonstrated in Fig. 3. Denote G' as the graph representing the topology of new

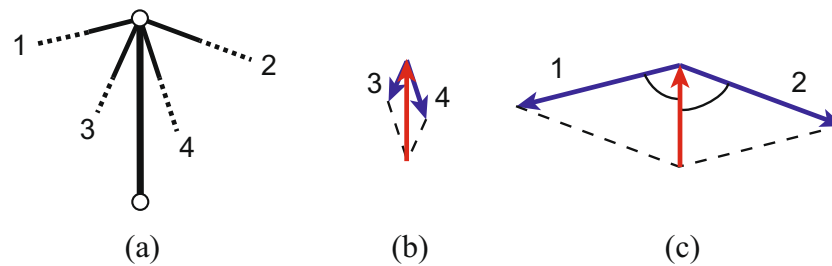


Fig. 2 Preference of larger angle between struts and cables by the objective function. **a** A vertex in the ground structure connecting one member that has already been selected to be a strut (shown with a solid line) and four candidate cable members (shown with dashed lines). For a given compression load in the strut, if cables 3 and 4 are selected

as in **b**, the sum of tension and the average angle between struts and cables are small. If cables 1 and 2 are selected as in **c**, the sum of tension and the average angle between struts and cables are large, which is preferred according to the objective function

solution \mathbf{F}' , which is a union of the original graph G and its symmetric images (i.e., $h_j(G)$). Thus, the new associated symmetry group (K') of G' expands to the same as H . Now, the new solution is clearly feasible, and $\min(\xi \mathbf{F}) \geq -1$, which means that the new solution might be able to be further maximized by a scalar $\xi > 1$ on G' . Therefore, we conclude that there is always a solution of full symmetry preserved from the input ground structure with larger or equal objective than any solution with less or no symmetry. The value of ξ depends on how much the compression field of the original solution overlaps with that of its symmetric images (under h_j 's). If there is no overlapping compression field, then $\xi = (m + 1)$. The level of overlapping is closely related to the symmetry number of the solution: a general observation is that the smaller the symmetry number is, the less overlapping. Thus, a solution with less symmetry is likely to have objective value much smaller than the possible optimum (with full symmetry) because ξ can be larger. In other words, for a force maximization problem, a solution with more symmetry is likely to yield a larger objective than the ones with less or no symmetry.

The above discussion about the relaxed LP problem helps us to gain some insights into the original discrete problem. As the topological constraint becomes active, the feasible domain of the new problem reduces to some discrete rays within the feasible cone of the relaxed LP problem. Each

of these rays represents a specific topology with a scalable self-equilibrating prestress field that satisfies the discontinuity constraint of struts. In other words, the feasible domain of the discrete optimization problem is a subdomain of that of the relaxed continuous problem. As we discussed in previous paragraphs, symmetric designs yield larger objective functions in the relaxed continuous design space. Because adding a topological constraint does not change the underlying mechanics, performing force maximization on a subset (i.e., the discrete feasible domain) of the relaxed feasible domain should have the same feature: if we sweep the discrete feasible domain to the increasing direction of the objective function, we conjecture that a symmetric solution is still likely to yield a larger objective. However, as we foresee, it is almost impossible that the optimal solution to the discrete problem would inherit all symmetries of the input ground structure. Indeed, as we observe from the numerical examples, an optimized tensegrity structure may possess many symmetries if the input ground structure is highly symmetric, but the symmetry number is usually smaller than that of the ground structure. That is to say, it is possible to obtain asymmetric solutions from symmetric ground structures.

We note here that our formulation is not concerned about finding tensegrities with a kinematically indeterminate dual truss. If mechanical performance is the preferred metric

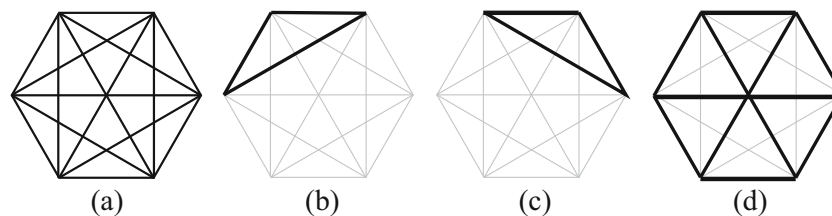


Fig. 3 **a** A symmetric planar ground structure. **b** A subset of the ground structure (representation of G) indicated by black solid lines. **c** Another subset of the ground structure (representation of $h_j(G)$) obtained by applying a symmetry operation of the ground structure to

the one shown in **b**. The structures in **b** and **c** are physically equivalent, as the relative relationships between the nodes and members remain unchanged. **d** An embedded structure that has the same symmetry group as the initial ground structure

over aesthetics, then kinematic indeterminacy is not a good choice of constraint in the design problem because it offers no benefits for stiffness and stability of the structure. This discussion also aligns with the last paragraph of Calladine's landmark paper (Calladine 1978): "On the other hand, if the aim is to design economical but stiff engineering structures it is not clear that there is much point in making the outer network so sparse that the resulting frame has a number of infinitesimal modes whose stiffness is necessarily low." Our method is able to produce tensegrity structures that are kinematically indeterminate as reported by the kinematic indeterminacy count in the manuscript. *We show that kinematic indeterminacy can be obtained by fine tuning the geometry of the ground structure* (see the example in Section 4.1).

3.2 Mixed integer linear programming reformulation

In the aforementioned formulation (2a), the force vector \mathbf{F} is unrestricted in sign. By splitting the force vector into two non-negative vectors and adding integer variables, the above formulation can be transformed equivalently to the following mixed integer linear programming (MILP) problem:

$$\max_{\mathbf{t}, \mathbf{c}, \mathbf{s}} \mathbf{1}^T (\mathbf{t} - \mathbf{c}) \quad (5a)$$

$$\text{s.t.} \quad \mathbf{B}(\mathbf{t} - \mathbf{c}) = \mathbf{0} \quad (5b)$$

$$\mathbf{G}\mathbf{s} \leq \mathbf{n} \quad (5c)$$

$$\mathbf{0} \leq \mathbf{t} \quad (5d)$$

$$\mathbf{0} \leq \mathbf{c} \leq \mathbf{s} \leq \mathbf{1} \quad (5e)$$

$$\mathbf{s} \in \mathbb{Z}^{N_{E_g}} \quad (5f)$$

In formulation (2), we replace the force vector \mathbf{F} with the difference of two non-negative vectors ($\mathbf{t} - \mathbf{c}$). This splitting leads immediately to the physical meaning that the vector \mathbf{t} corresponds to the tension forces and \mathbf{c} corresponds to the compression forces. Thus, we decouple the tension and compression field. The binary design variables \mathbf{s} indicate the presence of struts, serving to replace the non-differentiable function χ . The binary matrix \mathbf{G} is elaborated upon in Section 3.3.

While the objective function and most constraints are directly translated from formulation (2) to formulation (5), it is not obvious to see that constraints (5c) and (5e) ensure (2c). Based on $\mathbf{c} \leq \mathbf{s}$, we can see that $\mathbf{s} - \chi(\mathbf{F}) \geq \mathbf{0}$, because s_e can be 1 when the corresponding force (c_e) is 0 while $\chi(F_e)$ must be 0 when F_e is 0. Considering that all entries of \mathbf{G} are either 1 or 0, we find that,

$$\mathbf{G}(\mathbf{s} - \chi(\mathbf{F})) \geq \mathbf{0}, \quad (6)$$

thus,

$$\begin{aligned} \mathbf{G}\mathbf{s} \leq \mathbf{n} &\implies \mathbf{G}\mathbf{s} - \mathbf{G}(\mathbf{s} - \chi(\mathbf{F})) \leq \mathbf{n} \\ &\implies \mathbf{G}(\chi(\mathbf{F})) \leq \mathbf{n} \implies \sum_{e \sim v} \chi(F_e) \leq n. \end{aligned} \quad (7)$$

The proposed formulation has a natural and smooth relaxation to linear programming as we increase the allowed connectivity of struts, i.e., Class n . It is also observed that the proposed formulation is less computationally expensive than other similar formulations (Ehara and Kanno 2010; Kanno 2012, 2013a, b; Xu et al. 2016) for problems of similar size, probably due to the simplicity of the formulation. Additionally, relative to existing formulations, we consider much fewer discrete variables (the minimal number required to define a tensegrity). The disadvantage of our treatment is that we do not have control over the physical contact of cables with other cables or struts. However, from a practical point of view, cables are usually very thin and flexible members such that even if they touch other members, the influence on the structure is local. It is also easy to handle the contact, for example, by making a small hole in the strut that can be passed through by an intersecting cable. More importantly, other formulations for topology design of tensegrity have not demonstrated their ability to capture a variety of known tensegrities. In contrast, the present formulation is effective in attaining many of the known configurations, as illustrated in Section 4 and Appendix 1.

3.3 Matrix notation for the topological constraints

The discontinuity of compressive members is a signature of tensegrity structures, although the generalized definition of tensegrity allows relaxation of the discontinuity. It is well known that this topological constraint can be expressed as a linear inequality on the integer variables related to the presence of struts (Ehara and Kanno 2010; Kanno 2012, 2013a, b; Xu et al. 2016). For completeness, and also for the ease of numerical implementation, we explain the idea using matrix notation here. Let's define the incidence matrix \mathbf{G} based on the ground structure such that:

$$G_{ij} = \begin{cases} 1, & \text{if member } j \text{ is connected to node } i \\ 0, & \text{otherwise} \end{cases} \quad (8)$$

Thus, \mathbf{G} is an $N_{V_g} \times N_{E_g}$ binary matrix which contains the connectivity information, i.e., the topology, of a ground structure. The parameters N_{V_g} and N_{E_g} refer to the number of nodes and members in the ground structure. Each column of \mathbf{G} contains exactly two nonzero entries whose row indices correspond to the end nodes of a member. We then define a binary vector of size $N_{E_g} \times 1$, whose k th entry refers

to the k th member of the ground structure, with the value of 1 indicating the presence of a member. For any collection of members that are embedded in the ground structure, there exist a unique binary vector \mathbf{x} representing the collection. When we apply matrix vector multiplication as $\mathbf{G}\mathbf{x}$, the resultant vector is of size $N_{V_g} \times 1$, where each entry indicates the number of members connected to each node. Let us use the same vector \mathbf{s} as before for the collection of all compressive members. Then, the discontinuity condition is written as a linear constraint:

$$\mathbf{G}\mathbf{s} \leq \mathbf{n} \quad (9)$$

where \mathbf{n} is a $N_{V_g} \times 1$ vector of positive integers confining the level of discontinuity of the struts. For Class-1 tensegrity, we have that $\mathbf{n} = \mathbf{1}$. This idea is often used in the field of graph theory for matching problems (Godsil and Royle 2001). Indeed, this linear constraint reveals an interesting possibility when there are different connectivity constraints of struts at different nodes.

Considering practical construction of tensegrities, it is desirable to avoid physical contact of struts. One can address collisions between struts as a linear constraint about the integer design variables, similarly to the discontinuity constraint. Although there are ways to get around the case when two struts collide mid-length (e.g., splitting one strut near the collision point, or making struts curved), in practice, these intersections should be avoided because they make the tensegrity difficult to manufacture. To control collisions in the design, an additional topological constraint can be added that prevents the physical intersection of struts (Kanno 2013b). Suppose that we have a criterion that judges whether there is a conflict between two struts. For each (potential) intersection of members (i, j) in the ground structure, a (binary) row vector is defined, with ones in the column positions for members i and j , respectively. Sweeping the entire ground structure, we assemble these row vectors into a binary matrix \mathbf{G}_p , whose number of rows is the number of (potential) conflicting pairs. Then the physical constraint is written in the following form:

$$\mathbf{G}_p\mathbf{s} \leq \mathbf{1} \quad (10)$$

The matrix \mathbf{G}_p works following the same logic as the topological constraint matrix \mathbf{G} . Each row of \mathbf{G}_p corresponds to a fictitious intersection point reporting an occurrence of conflict between two members. For the case that several members intersect at the same point, as we impose the constraint using (10), a violation happens whenever two of the intersected members are present in the structure. In this paper, we set the collision criterion to be the intersection of centerlines of members. A different criterion can be found in Kanno (2013b). The number of rows of \mathbf{G}_p depends on the specific geometry of the ground structure. The construction of the matrix \mathbf{G}_p is conducted as

an offline process a priori to the optimization. Using parallel computing and other techniques from computer graphics, the process can be efficiently done.

It should be noted that this intersection test in our formulation does not involve the cables (tensile members), since they are not included in the vector \mathbf{s} . This follows from the assumption that the tensile members are thinner and typically flexible enough to handle intersections (collisions). Moreover, colliding cables can split at the intersection point creating a new node, with no effect on the principles and behavior of the tensegrity.

3.4 Ground structure method

A typical ground structure (Dorn et al. 1964; Smith 1998; Zhang et al. 2017) is a set of nodes and members within a fixed geometry, as illustrated by Fig. 4. In structural topology optimization, the ground structure method is particularly suitable for design of discrete structures (Bendsøe and Sigmund 2003). The importance of the geometry and layout of ground structures has not yet been discussed for topology design of tensegrity. As the main input to the optimization, the properties of the ground structures can have a big influence on the solution. For example, defining passive regions in the ground structure where no member can cross provides some control over the final tensegrity design. We adopt the techniques on ground structure generation developed for typical topology optimization, and explore how they can be used to tune the final design of tensegrities.

The ground structure can be generated inside arbitrary domains with various geometries. For convex domains, it is relatively easy to generate a geometrically conforming ground structure inside the domain. However, the challenge arises for ground structures filling concave geometries, in which members with both ends within the valid domain can have a part that is outside. We adopt the restriction zone idea from Zegard and Paulino (2015), which is inspired by the collision detection algorithm used in computational

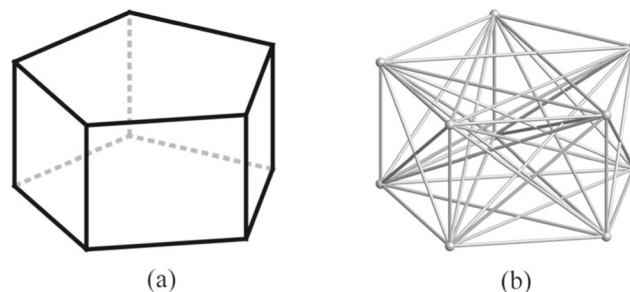


Fig. 4 The ground structure generated within pentagon prism. **a** Geometry of the pentagon prism. **b** The ground structure connecting every pair of nodes, which are located on the vertices of the prism

geometry, to resolve this issue. Members with any portion within the restriction zone are removed, resulting in a ground structure that conforms to the specified concave geometry.

We can control the length of members by further adjusting the ground structure, which may be useful, for example, if we want to avoid members that can easily buckle. If the constraint applies to both struts and cables, we simply remove the members from the ground structure that exceed the length limit. If the length constraint is only applicable to the struts, we impose a zero upper bound on the corresponding design variables in the vectors \mathbf{c} and \mathbf{s} . Notice that this strategy is only effective for unstructured ground structures without collinear members, which are typically used for topology design of tensegrity. When Class-1 tensegrity is used (emphasis of this paper), the “length constraint” is also effective for structured ground structures because no pair of collinear struts are allowed to connect to each other.

4 Numerical examples: verification and extension

In this section, we demonstrate that the proposed formulation is effective in reproducing known tensegrity structures by feeding specific geometries of the ground structure. Additionally, by varying the geometric parameters of the known tensegrities, we discover new forms of tensegrity. Hence, we provide a new perspective on the classification of tensegrity by its geometry rather than its topology.

For each example, numerical data is provided in tables. The numbers of nodes and members in the ground structure are denoted N_{V_g} and N_{E_g} , respectively. The terms N_V and N_E are the numbers of nodes and members in the final topology, respectively. The stability status of the obtained designs is also provided based on the criteria discussed in Section 2. The degree of kinematic indeterminacy (KI) of the dual truss of a tensegrity is also included in the

tables. We observe that for symmetric ground structures, the optimized solutions usually have one or more mechanisms associated with their dual truss. When a length limit for struts is applied, the number of reduced integer variables is given as N_I . The running time of MILP is reported as T_{opt} for reference.

We explore the categories of tower tensegrity and spherical tensegrity in this section. Other examples including prismatic tensegrity and symmetric star-shaped tensegrity can be found in Appendix 1. The physical constraint is applied to restrict the intersection of the centerlines of struts, using the method proposed in Section 3.3.

4.1 Tower tensegrity

The general composition of the geometry of tower tensegrity is shown in Fig. 5. We restrict our study to two-layer towers, in which two twisted prisms are aligned vertically with an overlapping height h_d . The angles α_1 and α_2 measure the twisting of the twisted prisms, and β is the relative rotation between the two prisms. Following this rule, by altering α_1 , α_2 , β , h_d , as well as the base polygon of the twisted prisms, we can find different embedded tensegrity structures.

One famous example in this category is the “Saddle-Vertical-Diagonal” (SVD) tensegrity (Sultan 1999). The geometry of the two-stage tower tensegrity can be obtained by laying one twisted triangular prism on top of another, as illustrated in Fig. 6a. To recover the specific configuration of the SVD tower tensegrity, the geometric parameters listed in Fig. 7a are selected to satisfy the formula given by Tibert (2002). The resulting tensegrity is plotted in Fig. 6b. The optimization selects 6 struts and 24 cables out of 66 candidate members in the ground structure within 0.06 s. The obtained tensegrity is known to have a dual truss with 1 degree of kinematic indeterminacy.

A free choice of the parameters leads to new tensegrities. For example, the designs shown in Fig. 7 are obtained based

Fig. 5 **a** The geometry and generation of the tower tensegrity. **b** Illustration of the cylindrical restriction zone adopted in this example. Any member in the initial ground structure that passes through this region is removed

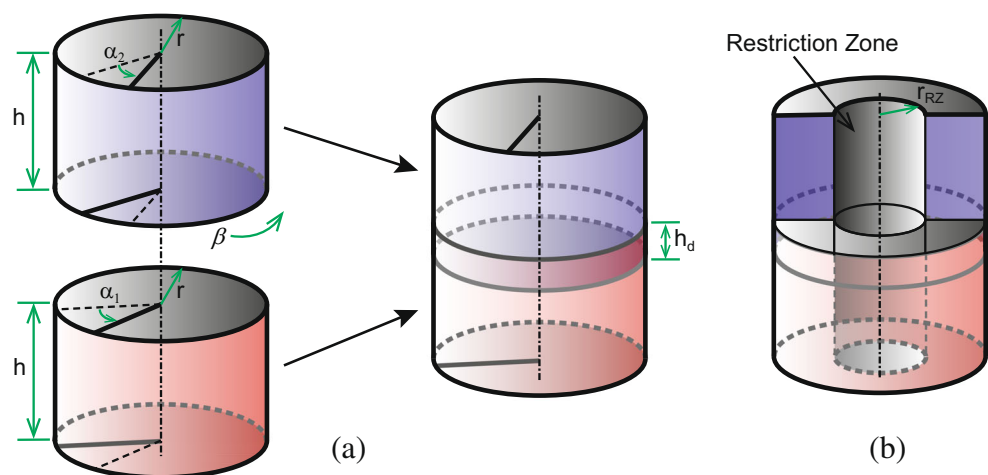
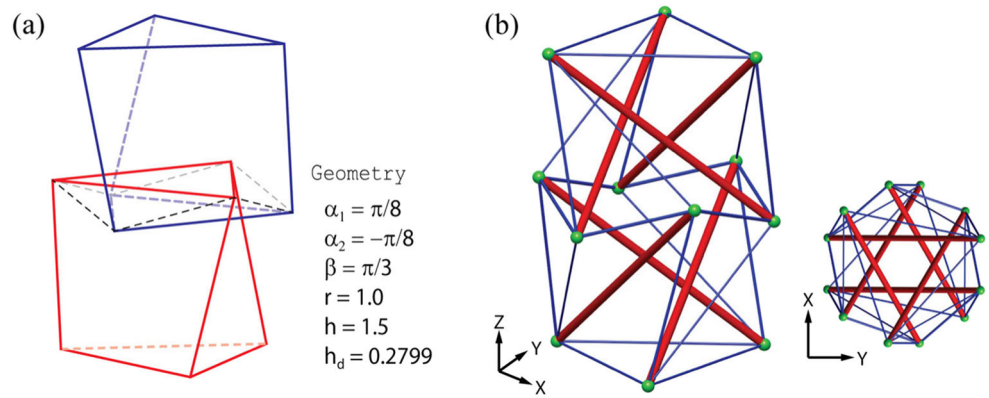


Fig. 6 The SVD tower tensegrity. **a** Geometric decomposition of the SVD tower, where the 12 vertices are the nodes used to generate the ground structure. **b** The design obtained using the proposed formulation, which recovers the known form of the SVD tower tensegrity



on hexagonal prisms with $\alpha_1 = \alpha_2 = \pi/8$ and $\beta = \pi/8$. We further show that by adding a hole in the ground structure and adding length constraints, we can tune the design to different configurations, as shown in Fig. 7c, d. If we adjust the overlapping depth h_d to be 0.283, the resulting tensegrity design becomes kinematically indeterminate—its dual truss has 7 infinitesimal mechanisms (see Fig. 7e). This example shows that the geometry of the ground structure is a crucial aspect in the topology optimization of tensegrity.

By fine-tuning the geometry of a ground structure, we can generate a family of tensegrities with different features. Information for all four designs is provided in Table 1.

4.2 Spherical tensegrity

Spherical tensegrity constitutes a large family among the known tensegrities. In this section, we will design tensegrities with nodes on a sphere. We will first recover

Fig. 7 Extended examples of tower tensegrity. **a** The basic geometry. **b** The design obtained directly from the ground structure generated with full connectivity. **c** The tensegrity obtained by limiting the length of struts to 2.5, which is in consistent units with the dimension of the geometry. **d** In addition to length limit, a cylindrical restriction zone is applied with $r_{RZ} = 0.3$. **e** Based on **d**, by adjusting the overlapping height h_d , a kinematically indeterminate tensegrity design emerges naturally as a result

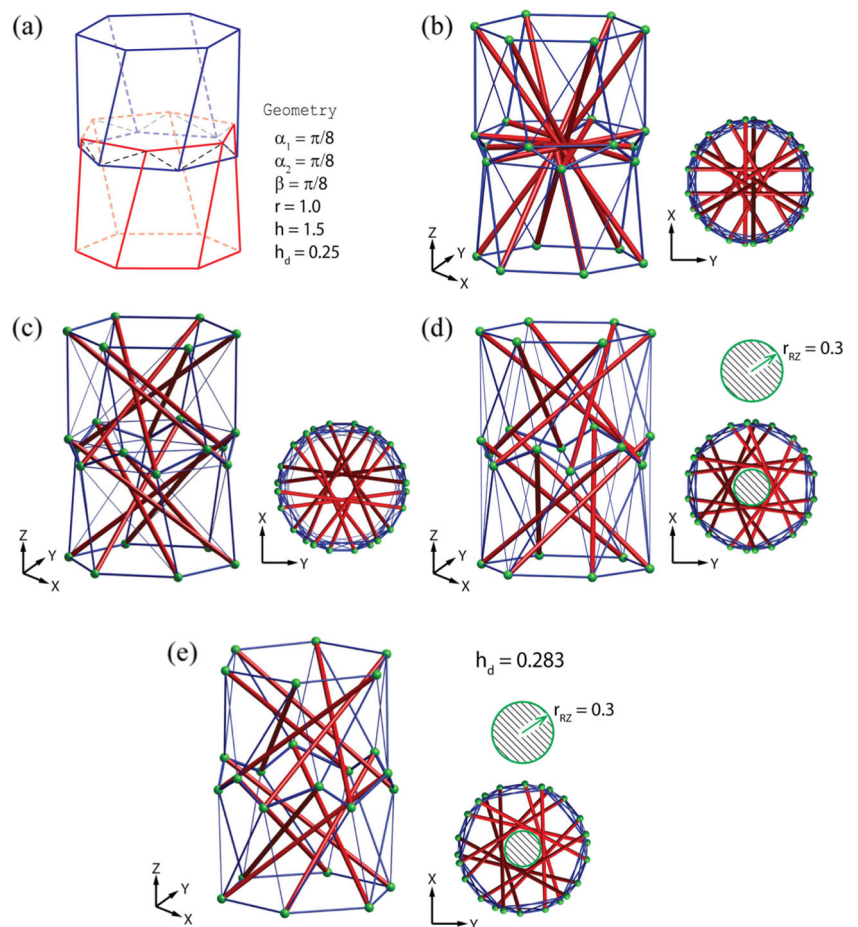
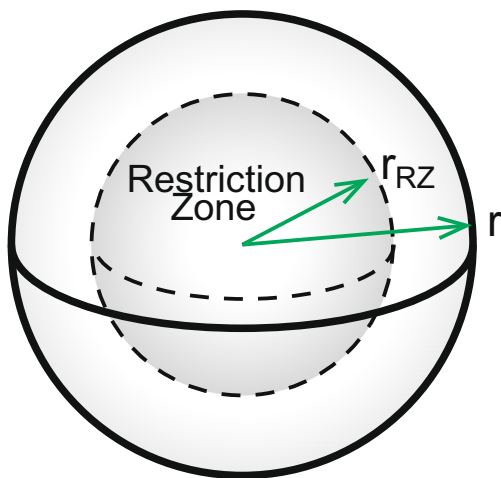


Table 1 Computational results for designs shown in Fig. 7

Design	N_{V_g}	N_{E_g}	N_V	N_E	N_I	Obj.	KI	Stability	T_{opt}
(b)	24	276	24	72	276	22.23	0	Super-stable	0.43 s
(c)	24	276	24	72	240	22.03	0	Super-stable	0.16 s
(d)	24	228	24	72	198	19.47	0	Super-stable	0.20 s
(e)	24	228	24	60	198	19.61	7	Prestress-stable	0.09 s

some of the designs that are already known. Then, we propose some new designs obtained by the proposed method. We will adopt the restriction zone method to generate ground structures with a central hollow ball region. This can be useful for tensegrity robots or protectors design in which a central void may need to contain some functional devices (Caluwaerts et al. 2014). The geometry of the restriction zone for this example is illustrated in Fig. 8. The nodes are on the outer sphere and an inner ball with radius r_{RZ} is defined as the restriction zone.

The known spherical tensegrity structures often outline regular polyhedrons or truncated regular polyhedrons. We present three such structures that are reproduced by the proposed formulation, as shown in Fig. 9a–c. The outline polyhedrons are icosahedron, dodecahedron, and cuboctahedron. The first one (Fig. 9a) relies on a ground structure generated based on the vertices of an icosahedron, with a restriction ball of radius $r_{RZ} = 0.2$. The second tensegrity (Fig. 9b) has cables on the surface of a dodecahedron. The restriction zone for the ground structure has a radius $r_{RZ} = 0.5$. The last one shown in Fig. 9c is a Class-2 tensegrity, in which at most two struts can connect at each node. There are four triangles of struts in this tensegrity, and each of the closed chain of struts are named “strut circuits” by Motro (2006). The initial ground structure for this one has no restriction zone. Quantitative data is provided in Table 2.

**Fig. 8** Illustration of the ball-shaped restriction zone adopted in this example

By taking different point sets on a sphere, we discover new tensegrities. Figures 10, 11, 12, and 13 list some of the new designs of tensegrity that have been discovered by the proposed formulation. For some of them, restriction zones are used. The first one shown in Fig. 10a outlines a small rhombicuboctahedron. The one in Fig. 10b comes from the truncated icosahedron, which is usually known as the “Bucky ball.” There is an existing design of tensegrity (Li et al. 2010a) that looks similar to the geometry of a truncated icosahedron, but their nodes are not exactly at the vertices of the polyhedron, and the topologies are also different from the one we obtained. The tensegrity shown in Fig. 11a is obtained as the best candidate optimal solution when the optimization hits the time limit. The realization of this design is shown in Fig. 11b. We also construct a model, which is shown in Fig. 12b, based on the design shown in Fig. 12a. The structure shown in Fig. 13b is a Class-2 tensegrity embedded in the geometry of an icosahedron, in which the struts make a single loop of circuit. Quantitative data is provided in Table 3.

5 Free-form design

In this section, we seek tensegrities that conform to arbitrary non-regular geometries, which is desirable for designing tensegrities for real applications.

5.1 Double-layer tensegrity dome

Tensegrities are sometimes used for roof structures (Hanaor and Liao 1991; Pellegrino 1992). In this section, we will show a cylindrical dome design obtained by solving the proposed optimization formulation. The design domain is shown in Fig. 14a. The ground structure is generated on 54 grid points placed on the surface of the design domain. The members are all confined in the design domain by applying a restriction zone in the interior of the inner cylinder.

The optimization takes 97.61 s to converge. We impose Class-1 discontinuity constraint (i.e., $n = 1$) and prohibit the collision of the centerlines of struts. There is no length limit on the members. A posteriori structural analysis shows that obtained tensegrity is super-stable, and its dual truss is not infinitesimally rigid.

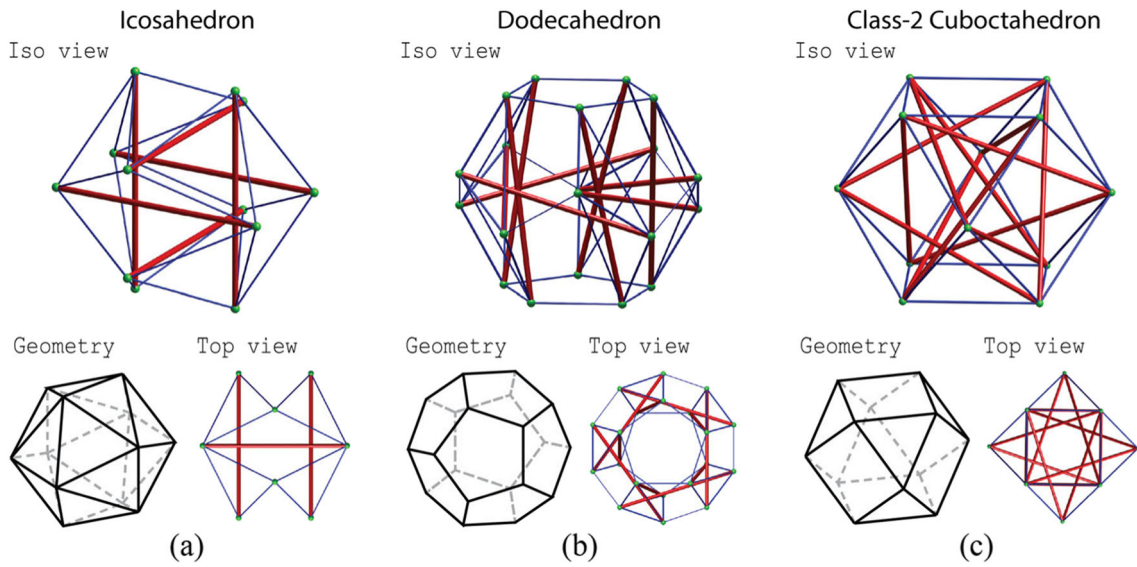


Fig. 9 Some known spherical tensegrities that are reproduced. The ground structure of design (a) has a restriction zone with $r_{RZ} = 0.1$, design (b) has a restriction zone with $r_{RZ} = 0.5$, and no restriction zone is used in design (c)

Table 2 Computational results for designs shown in Fig. 9

Design	N_{V_g}	N_{E_g}	N_V	N_E	Obj.	KI	Stability	T_{opt}
(a)	12	60	12	30	3.80	1	Super-stable	0.01 s
(b)	20	150	20	50	30.18	5	Super-stable	0.50 s
(c)	12	66	12	36	32.78	1	Super-stable	<0.01 s

Fig. 10 New examples of spherical tensegrities obtained using the proposed method. The radii of the restriction zones as defined in Fig. 8 are as follows: **a** $r_{RZ} = 0.20$, **b** $r_{RZ} = 0.65$

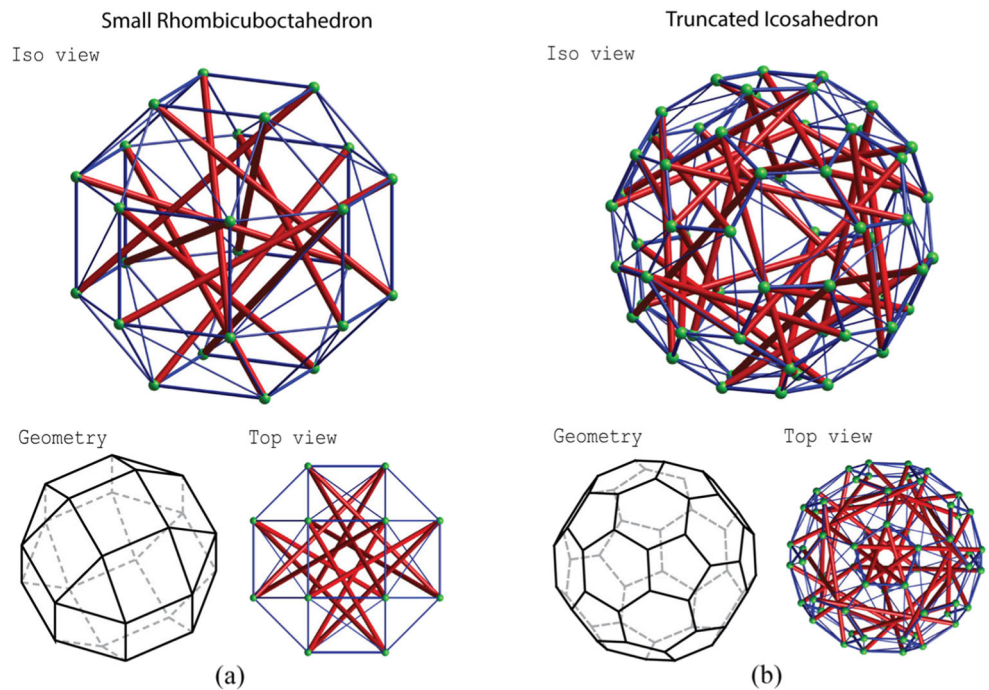


Fig. 11 A tensegrity that outlines a small rhombicosidodecahedron. **a** Digital rendering of the obtained design, using restriction zone with radius $r_{RZ} = 0.70$. **b** A physical model made of wood struts and 3D printed cables. The cables are printed with a rubber-like material known as Ninja Flex

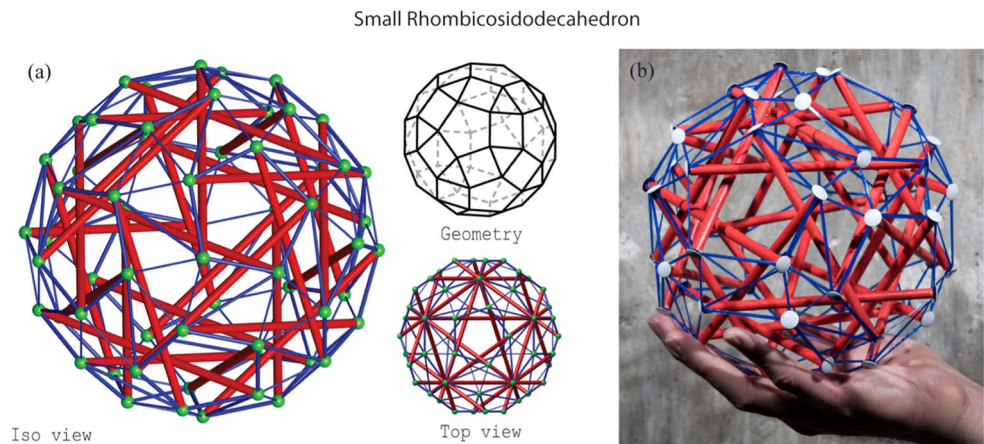


Fig. 12 A spherical tensegrity optimized from a ground structure generated based on 16 uniformly distributed points on the unit sphere and no restriction zone. **a** Digital rendering of the obtained design. **b** The physical model made of wood struts and rubber band cables

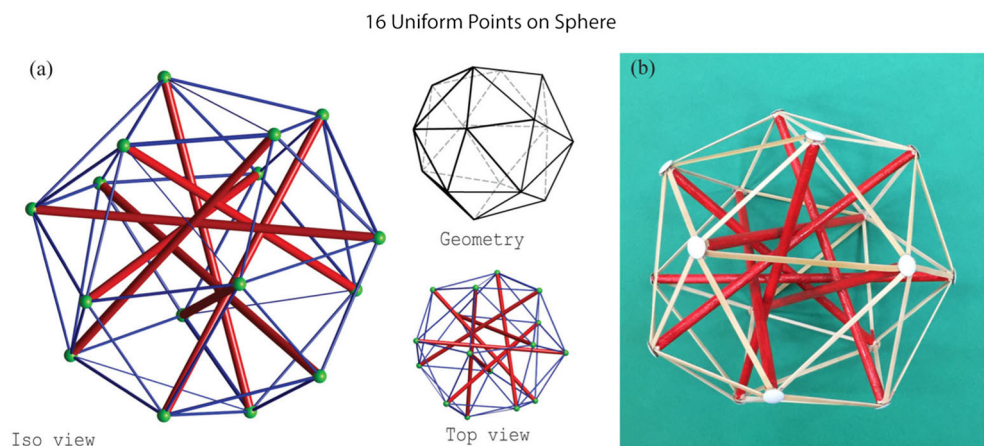


Fig. 13 Other new designs of spherical tensegrities obtained using the proposed method. **a** A dense tensegrity that has 120 nodes uniformly placed on a sphere and restriction zone with radius $r_{RZ} = 0.65$. **b** A Class-2 tensegrity that has a continuous loop of struts

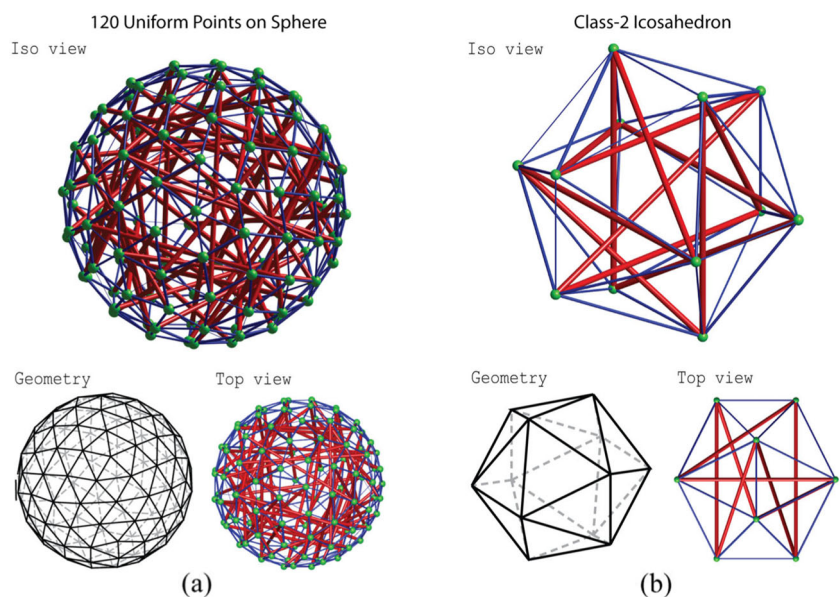


Table 3 Computational results for designs in Section 4.2

Design	N_{V_g}	N_{E_g}	N_V	N_E	Obj.	KI	Stability	T_{opt}
Figure 10a	24	264	24	72	18.24	1	Super-stable	0.53 s
Figure 10b	60	990	60	180	74.26	3	Super-stable	640 s
Figure 11	60	870	60	180	55.27	0	Prestress-stable	43,200 s
Figure 12	16	120	16	50	8.99	0	Super-stable	0.03 s
Figure 13a	120	4108	120	414	202.08	0	Super-stable	706 s
Figure 13b	12	66	12	42	7.55	0	Super-stable	< 0.01 s

Fig. 14 Design of a Class-1 cylindrical double-layer tensegrity dome. **a** The design domain: $L = 3$, $R_o = 1$, $R_i = 0.7$. The initial ground structure has 54 nodes and 882 members. **b–d** Different views of the obtained tensegrity. The design contains 54 nodes, 27 struts, and 153 cables. The dual truss of the tensegrity has 2 first-order mechanisms (KI = 2). The tensegrity structure is super-stable

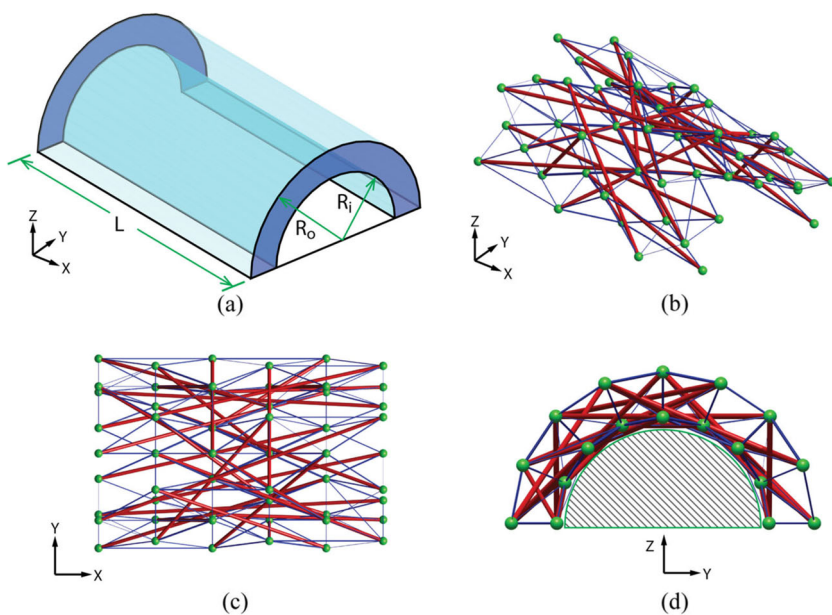


Fig. 15 Different views (a–c) of Taubin’s heart. The mesh nodes are used to generate the ground structure

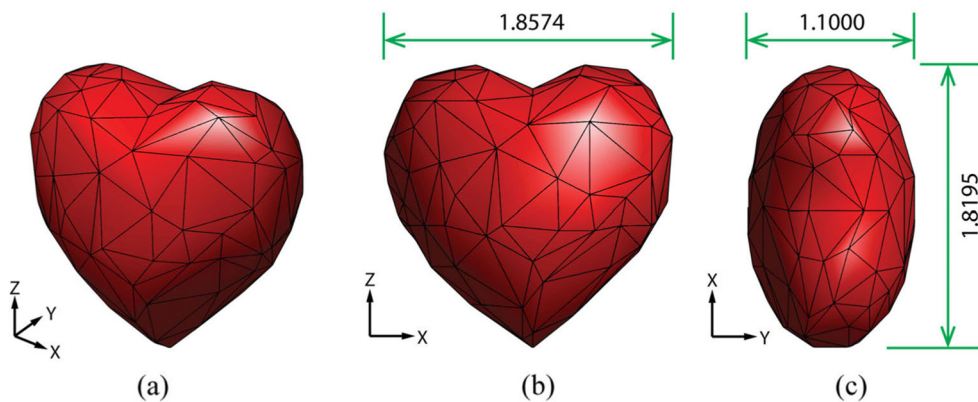
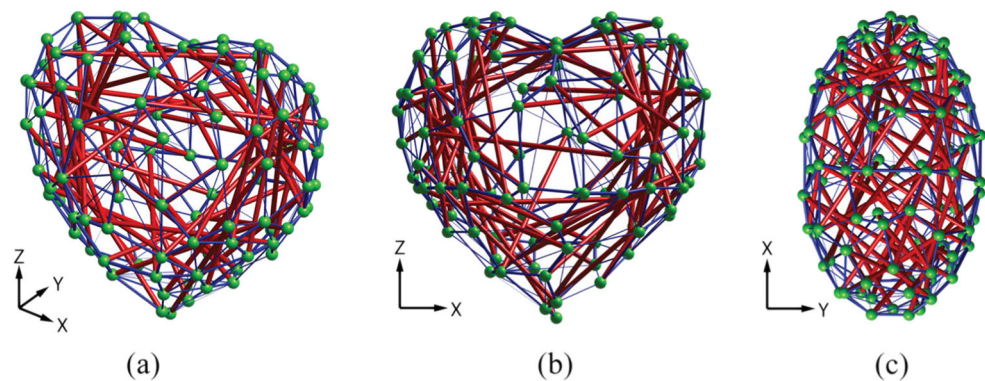


Fig. 16 Different views (a–c) of the tensegrity which outlines the Taubin’s heart. The tensegrity contains 53 struts and 312 cables. The lengths of the struts are limited to 1.2, with consistent units to the dimensions of heart surface. Structural analysis shows that the structure is super-stable



5.2 Taubin’s heart

Here, we design a tensegrity structure with Taubin’s heart shape (Taubin 1994). The shape of the surface is defined by a level set:

$$\left(x^2 + \frac{9}{4}y^2 + z^2 - 1\right) - x^2z^3 - \frac{9}{80}y^2z^3 = 0 \quad (11)$$

where x , y , and z are the Cartesian coordinates in \mathbb{R}^3 . The size is scaled uniformly such that the heart surface has the dimensions shown in Fig. 15. Then, a triangular mesh is generated on the surface that contains 107 nodes and 210 faces. The ground structure is generated based on the nodes of the mesh without restriction zones. We forbid the intersection of centerlines of struts and constrain the lengths of the struts to be smaller than 1.2, in consistent units with the size of the heart surface.

The obtained tensegrity is shown in Fig. 16, which takes 9032 s to converge. The tensegrity has 53 struts and 312 cables, optimized from 5671 candidates, among which $N_I = 3282$ members are potential struts. One of the nodes in the initial ground structure is ignored as no member is connected to it. The tensegrity has an infinitesimally rigid dual truss, ensuring prestress stability. Its geometrical stiffness matrix is also positive semi-definite, indicating it is super-stable.

6 Numerical aspects: implementation and efficiency

The numerical implementation of the formulation is memory efficient. All of the constraint matrices can be constructed and stored in a compressed format as sparse matrices. Furthermore, the topological constraint and physical constraint matrices are binary. The bottleneck for the efficiency of the approach is the integer restrictions of design variables \mathbf{s} .

The basic algorithm for MILP is the branch-and-bound method. Advanced implementations usually adopt strategies

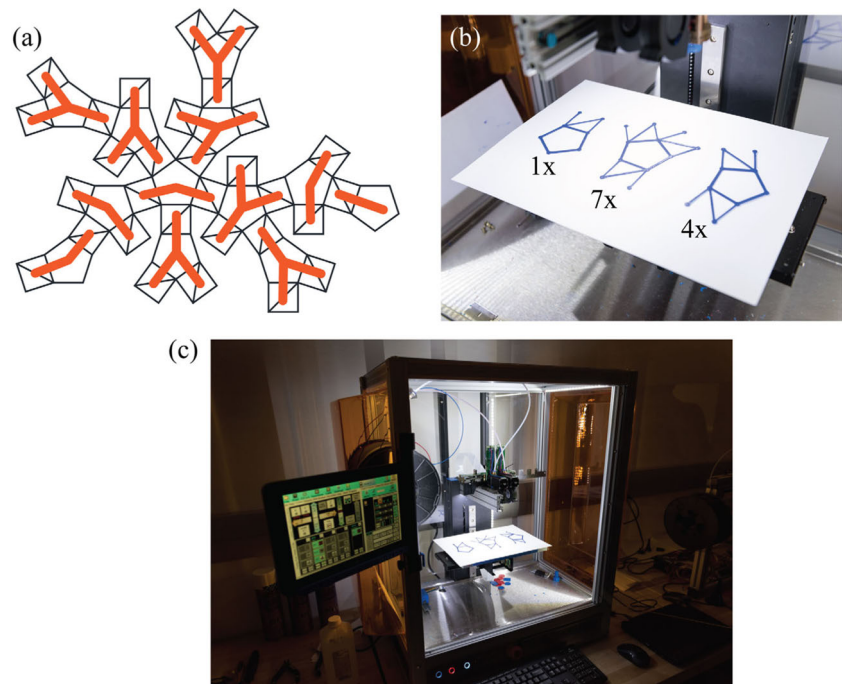
such as presolve and cutting-planes to reduce the problem size, and heuristics and parallelism to speed up the branching search. The fundamental idea is to relax and branch the MILP problem to many LP relaxations by allowing the discrete integer variables to become continuous. In each branch-and-bound search, the subproblem is solved as an LP problem. If there is an optimal solution of the LP relaxation found during the branching process that satisfies the integer restrictions, then we have found a feasible candidate optimal solution to the original MILP.¹

Note that, the problem posed by our proposed formulation does not guarantee existence of a solution. The existence of a nontrivial optimal solution depends on the number of bars in the ground structure and the geometry of the ground structure. However, usually we can find a solution for a dense ground structure.

Additionally, as we observe from the examples, the computational cost of the MILP varies significantly from problem to problem and does not only depend on the problem size. This is because, for some problems, an optimal integer solution might appear at an early stage of the branching process. Therefore, the time that the optimization needs to converge is highly problem dependent. A larger size problem might be solved within less time than a smaller size problem (for example, the designs shown in Figs. 11 and 13a). In addition, the authors remark that it is not always necessary to find a strictly converged solution. If the solving time is limited, it is fine to accept a feasible suboptimal solution, like the case of Fig. 11. However, we observe that the implementation of the proposed formulation is generally more efficient than other MILP formulations in the literature (Ehara and Kanno 2010; Kanno 2012, 2013a, b), based on computational time comparisons for problems with ground structures of similar complexity.

¹The examples in this paper are solved by the optimization software Gurobi 6.5 (Gurobi Optimization 2014) executed by a MATLAB code. The code is operating on a desktop with an 8-core 3.0 GHz Intel Xeon CPU. It is also possible to use other solvers such as the MATLAB built-in function “intlinprog” to solve the problem.

Fig. 17 **a** The thin black lines show the flattened cable net. The thick orange lines mark the 12 pieces that are printed separately. **b** The printed pattern pieces. The number on the side of each pattern indicates the number of times that this pattern embedded in the whole cable net. **c** HYREL 3D printer producing the elastic cable nets. Image courtesy: Rob Felt



7 Fabrication of the tensegrity models aided by additive manufacturing

In this section, we will briefly describe the fabrication process for the physical model shown in Fig. 11b. For such a complex design, it is difficult to attain the required prestress by connecting the cables one-by-one to the struts. Ideally, we want to make the cable net as a whole piece of network. However, the cable net outlines a polyhedron, and it is very difficult to print such three-dimensional frame-like structures with the soft material that we are using. Therefore, we decompose the three-dimensional cable net into 12 planar pieces, each containing a pentagon, as shown in Fig. 17a. Actually, the 12 pieces are made from only three different patterns (7 of one pattern, 4 of the second pattern, and 1 of the third pattern) as shown in Fig. 17b. By printing 12 flat pieces, there is no need to print a supporting scaffold, which makes the printing process significantly easier than for the full, 3D cable net. The cable net pieces were fabricated using the fused filament fabrication (FFF) technology on a HYREL 3D printer.² The material of the filament is called Ninjaflex,³ which is a rubber-like soft material that can sustain large elastic deformations. The cross-sectional areas of the cables

are determined proportionally to the magnitudes of the designated prestress forces. Furthermore, there are at most two pieces of cable net connected to one node, which leads to an easy and clean assembly process of the tensegrity structure using the printed cable components and the wood rods (0.25 in. diameter). The fabrication precision is also easy to control using the 3D printer as compared to making all the components by hand.

With the help of additive manufacturing, making complex tensegrity models (desktop size), which is usually a difficult task, becomes a relatively easy procedure as described in this section. Thus, researchers and designers can quickly prototype their tensegrity designs. Moreover, such an approach can have a positive impact on engineering education. For instance, 3D printing the tensegrity models designed using our topological optimization approach is a means to bring the computational design to reality, which motivates students to design their own tensegrities and add a new dimension to their learning, so that the learning spans from the mathematical formulation, to the computational modeling, and to the fabrication.

8 Conclusion

In this paper, we have proposed a topology optimization formulation for the design of tensegrity structures based on the ground structure method and a MILP approach. The formulation is simple, elegant, and easy to implement.

²System 30M, HYREL 3D Inc, Norcross, GA, USA

³NINJATEK, Manheim, PA, USA

During optimization, a tensegrity is extracted from the many potential members in a ground structure by maximizing the summation of self-equilibrating forces. The obtained tensegrity design satisfies the self-equilibrium condition and the discontinuity condition of compressive members.

The effectiveness of the formulation is verified by numerical examples. The reproduction of existing well-known tensegrities is important because it shows that, as long as the specific geometry is provided, the proposed formulation, although simple, automatically converges to the desired solutions. The topology design of tensegrity is an open problem without a naturally defined objective; thus, the choice of the objective function can make a big difference. In this context, the force maximization formulation appears with some nice features. Although not enforced explicitly, the formulation usually leads to tensegrity structures that are stable and symmetric, which are commonly desirable features. We also explore the possibility to obtain tensegrities with desired geometrical and topological features by controlling the design space offered by the ground structure. This feature could be very useful when designing for engineering applications, in which the tensegrity structures must adapt their shapes in order to carry payloads or avoid nearby objects. The numerical implementation of our formulation is efficient in comparison to other mixed integer formulations and enables designs of relatively complex tensegrities, as shown in some of the examples. These benefits make it suitable for preliminary designs of engineering tensegrity structures (e.g., tensegrity protectors carrying a payload).

We remark that the formulation presented here is a basic one that can incorporate other constraints for different purposes. For instance, examples of constraints previously reported can be found in Ehara and Kanno (2010), Kanno (2012, 2013a, b), and Xu et al. (2016), which are also applicable, with some modifications, to our basic formulation. In future development, we plan to adopt some strategies such as a multi-step optimization (Felix and Vanderplaats 1987), to allow flexibility on the position of nodes so that we can combine the advantages of both topology and geometry design methods for tensegrity.

Acknowledgements The authors would like to extend their appreciation to Dr. Tomas Zegard and Ms. Emily D. Sanders for helpful discussions which contributed to improve the present work and to Mr. Rob Felt for taking photos of the physical models.

Funding information This study received support from the US NSF (National Science Foundation) through Grants 1538830 and 1321661. In addition, Ke Liu received support from the China Scholarship Council (CSC). We are grateful to the support provided by the Raymond Allen Jones Chair at the Georgia Institute of Technology.

Compliance with ethical standards

Disclaimer The information presented in this paper is the sole opinion of the authors and does not necessarily reflect the views of the sponsoring agencies.

Appendix 1: On reproducing known tensegrities: a verification study

One of the most well-known types of tensegrity is the prismatic tensegrity. This type of tensegrity has various configurations, but all of them obey the dihedral symmetry. A systematic study of the configuration and stability of the prismatic tensegrity can be found in the literature (Ohsaki and Zhang 2015; Zhang et al. 2009). The nodes of a prismatic tensegrity are located on the vertices of a twisted prism with each base face being a regular N -gon. The N vertices of the N -gon are incident on a circle. The twisting angle between the two parallel base faces is denoted as α , as shown in Fig. 18.

We first generate the ground structure based on the twisted prism with full connectivity between nodes. The prism has a height of 1.0 (i.e., $h = 1$), and the radius of the outline circle of the base polygon is also 1 (i.e., $r = 1$). The results are shown in Fig. 19 for different geometries of the twisted prism. All of the results are super-stable, which has been proved analytically by Ohsaki and Zhang (2015) and Zhang et al. (2009).

There is another family of tensegrity that has similar configurations to the prismatic tensegrities, namely the symmetric star-shaped tensegrity (Zhang and Ohsaki 2015), which also satisfies the dihedral symmetry. The difference is that a star-shaped tensegrity structure has two additional nodes lying

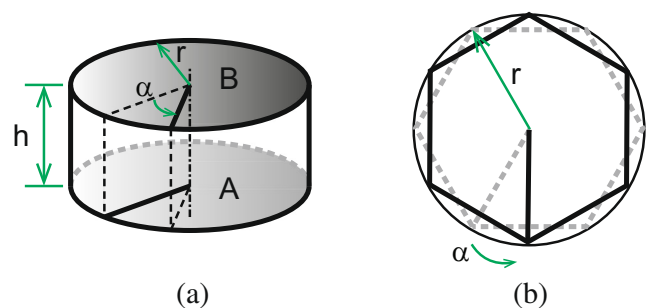


Fig. 18 The geometry and generation of a twisted prism. **a** The base polygon laid on the top circle B is obtained by rotating the same polygon on the bottom circle A with an angle α . **b** The top view of the twisting of the hexagonal base

Table 4 Computational results for the designs shown in Fig. 19

Design	N_{V_g}	N_{E_g}	N_V	N_E	Obj.	KI	Stability	T_{opt}
(a)	6	15	6	12	1.31	1	Super-stable	< 0.01 s
(b)	8	28	8	16	2.21	3	Super-stable	< 0.01 s
(c)	10	45	10	20	4.67	5	Super-stable	0.02 s
(d)	12	66	12	24	6.66	7	Super-stable	0.02 s
(e)	16	120	16	32	13.44	11	Super-stable	0.02 s
(f)	32	496	32	64	63.54	33	Super-stable	0.58 s

on the centroids of the base faces. Therefore, in a prismatic tensegrity structure, there is essentially only one type of node, but in a star-shaped tensegrity, there are two types of nodes. To reproduce the known star-shaped tensegrities, we

generate the ground structure using the nodes on the vertices of the twisted prism and the two additional nodes at the centroids of the top and bottom faces. Figure 20 shows a few examples of reproduced star-shaped tensegrities.

Fig. 19 Examples of prismatic tensegrities that are reproduced using the proposed method. Different base polygons are used to generate the twisted prism geometries: **a–f** For N -gon-based twisted prism, $\alpha = \pi/N$ if N is even, and $\alpha = \pi/2N$ if N is odd. Quantitative data is provided in Table 4

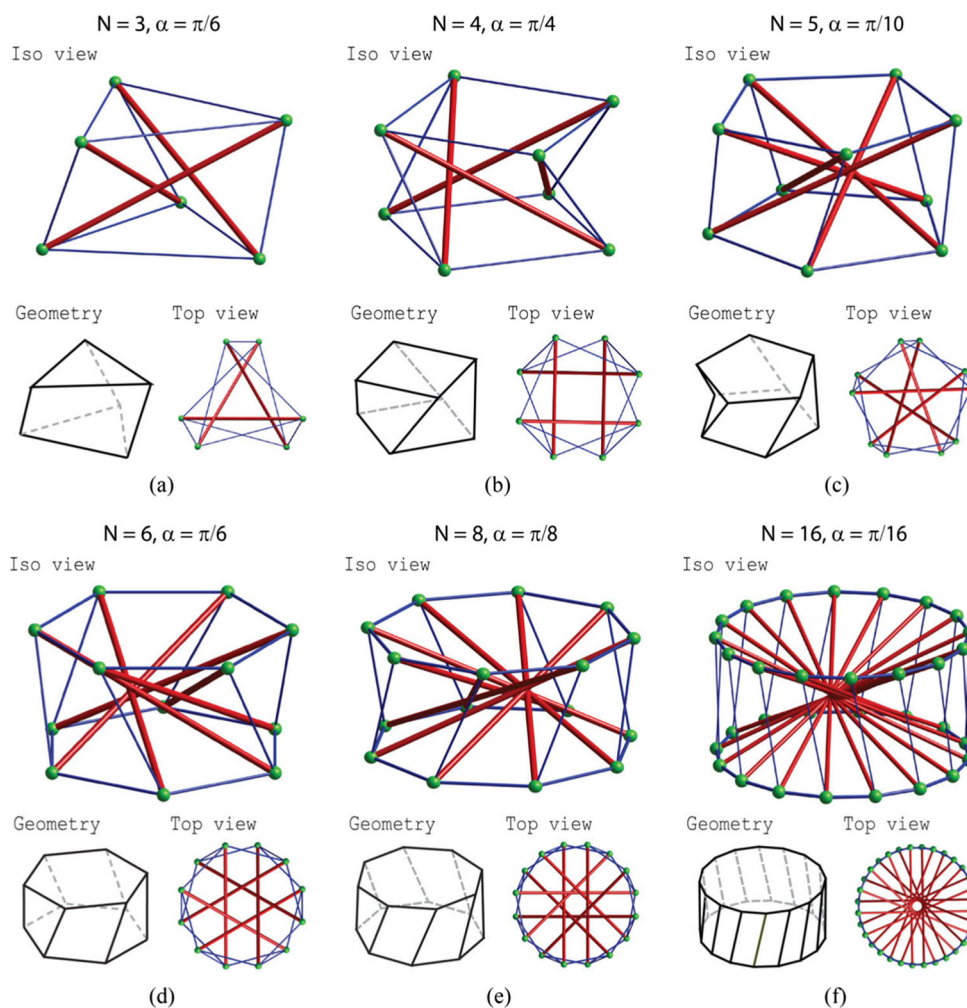


Fig. 20 Examples of star-shaped tensegrities that are reproduced using the proposed method. Different base polygons are used to generate the twisted prism geometries: **a–c** Compared to the prismatic tensegrities, the initial ground structures have two more nodes that are located at the centroids of the two base polygons. Quantitative data is provided in Table 5

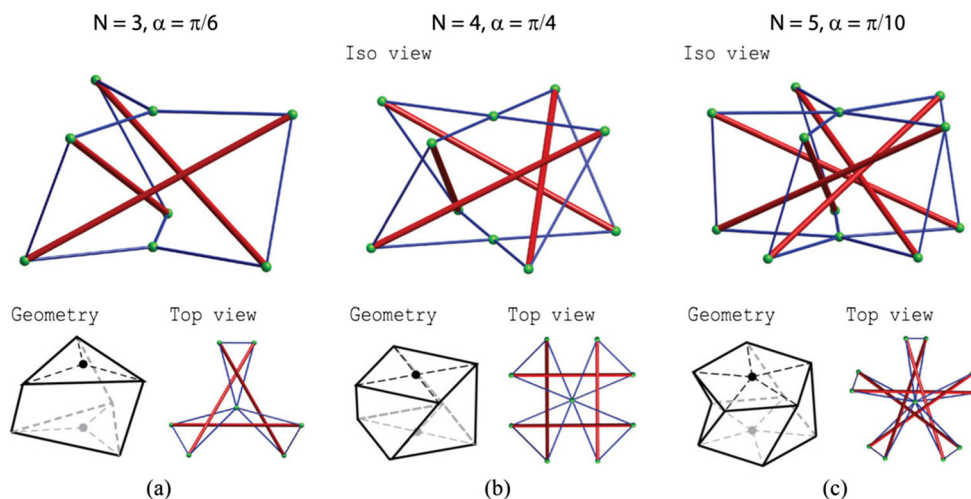


Table 5 Computational results for designs shown in Fig. 20

Design	N_{V_g}	N_{E_g}	N_V	N_E	Obj.	KI	Stability	T_{opt}
(a)	8	28	8	12	3.33	7	Super-stable	< 0.01 s
(b)	10	45	10	16	3.78	9	Super-stable	< 0.01 s
(c)	12	66	12	20	5.96	11	Super-stable	0.01 s

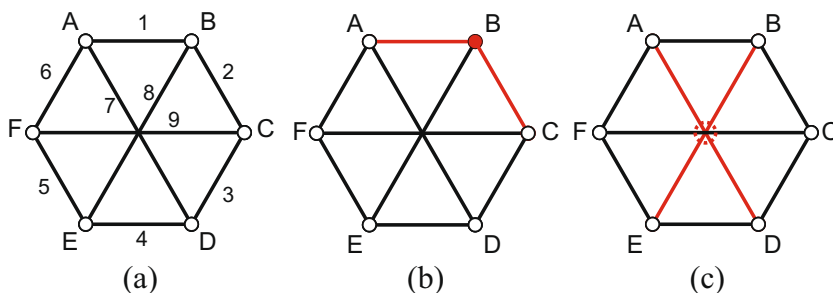
Appendix 2: An illustrative example of the topological constraints

We use the following example to illustrate how the topological constraint and physical constraint work. Suppose we have a ground structure as shown in Fig. 21a. Label the vertices from A to F and edges from 1 to 9. Based on the given topology, we can construct the topological constraint matrix \mathbf{G} as:

$$\mathbf{G} = \begin{bmatrix} 1 & 0 & 0 & 0 & 0 & 1 & 1 & 0 & 0 \\ 1 & 1 & 0 & 0 & 0 & 0 & 0 & 1 & 0 \\ 0 & 1 & 1 & 0 & 0 & 0 & 0 & 0 & 1 \\ 0 & 0 & 1 & 1 & 0 & 0 & 1 & 0 & 0 \\ 0 & 0 & 0 & 1 & 1 & 0 & 0 & 1 & 0 \\ 0 & 0 & 0 & 0 & 1 & 1 & 0 & 0 & 1 \end{bmatrix}_{6 \times 9} \quad (12)$$

The rows of the matrix correspond to the connectivity information at nodes A to F. The columns contain the connectivity

Fig. 21 **a** A simple ground structure with 6 nodes and 9 members. **b** The collection of members 1 and 2 in the ground structure. The two members are connected at node B. **c** Members 7 and 8 are contacting each other in the middle, indicating a conflict in space



information of members 1 through 9. For example, the third row shows that members 2, 3, and 9 are connected to node C. Furthermore, since members 7, 8, and 9 intersect at one point, we have the physical constraint matrix \mathbf{G}_p reads:

$$\mathbf{G}_p = \begin{bmatrix} 0 & 0 & 0 & 0 & 0 & 0 & 1 & 1 & 0 \\ 0 & 0 & 0 & 0 & 0 & 0 & 0 & 1 & 1 \\ 0 & 0 & 0 & 0 & 0 & 0 & 1 & 0 & 1 \end{bmatrix}_{3 \times 9} \quad (13)$$

As discussed before, the coincident intersection point is split into three fictitious intersection points.

Suppose we have a collection of members from the ground structure represented by the binary vector \mathbf{x} whose k th entry reflects the presence of member k in the collection. Let $\mathbf{x}_1 = [1, 1, 0, 0, 0, 0, 0, 0, 0]^T$ meaning that members 1 and 2 are in the collection as shown in Fig. 21b. The matrix vector multiplication $\mathbf{G}\mathbf{x}_1$ gives $[1, 2, 1, 0, 0, 0]^T$ which clearly shows that there are two members in the collection connected to node B. If the constraint is set for Class-1 tensegrity and the collection \mathbf{x}_1 represents the struts, \mathbf{x}_1 will violate the topological discontinuity constraint. To show how the physical constraint works, we set $\mathbf{x}_2 = [0, 0, 0, 0, 0, 0, 1, 1, 0]^T$, which contains members 7 and 8, as shown in Fig. 21c. The linear operation $\mathbf{G}_p\mathbf{x}_2$ produces $[2, 1, 1]$ with first component larger than 1 indicating a

violation. Thus, the physical constraint successfully shows that members 7 and 8 cannot exist at the same time.

Appendix 3: Basic structural analysis of tensegrity structures

The construction of the stiffness matrix for a tensegrity structure is different from a normal truss due to the presence of prestress forces. Detailed derivations and discussions can be found in Guest (2006, 2011) and Zhang and Ohsaki (2015). Here, we briefly summarize the key ideas. The basic assumptions here are that both struts and cables are rectilinear members made of materials that have linear elastic constitutive relationships, and the strains in the members are always small. The geometric stiffness matrix formulation adopted here is an incomplete version that is accurate for small strain analysis. Indeed, the present expression for \mathbf{K}_G is called the “stress matrix” (Connelly 1999), which is part of the complete geometric stiffness matrix (Guest 2011).

Assume the cross-sectional area, length, and Young’s modulus of member i are A_i , L_i , and E_i , respectively. The coordinates of node j are stored in the vector \mathbf{p}_j . First, let us define the modified incidence matrix \mathbf{C} . In graph theory, the incidence matrix is binary (like the matrix \mathbf{G} in (5c)), but here, the modified matrix is composed of 0’s, 1’s, and -1 ’s. Suppose member i links nodes a and b . Then, \mathbf{C} is defined as:

$$C_{ij} = \begin{cases} 1, & \text{if member } i \text{ is connected to node } j, \text{ and } j = a \\ -1, & \text{if member } i \text{ is connected to node } j, \text{ and } j = b \\ 0, & \text{otherwise} \end{cases} \tag{14}$$

The size of the modified incidence matrix \mathbf{C} is $N_E \times N_V$. Then, the augmented incidence matrix that connects the degrees of freedom to the members is defined as:

$$\mathbf{C}_{aug} = \mathbf{C} \otimes \mathbf{1}_{1 \times 3} \tag{15}$$

where \otimes means the Kronecker product, so that \mathbf{C}_{aug} has size $N_E \times 3N_V$. The vector $\mathbf{1}$ is a vector of ones. The total number of degrees of freedom in the structure is $3N_V$ because we are considering three-dimensional space. We assemble all the nodal coordinates (i.e., \mathbf{p}_j ’s) in a vector \mathbf{p} by blocks of 3 components. We obtain the equilibrium matrix as:

$$\mathbf{B} = \mathbf{P}\mathbf{C}_{aug}^T\mathbf{L}^{-1} \tag{16}$$

where $\mathbf{P} = \text{diag}(\mathbf{p})$, with its diagonal entries containing all the nodal coordinates, and \mathbf{L} being a diagonal matrix of

member lengths. We define another diagonal matrix \mathbf{D} of size $N_E \times N_E$, such that

$$D_{ii} = \frac{E_i A_i}{L_i} \tag{17}$$

Then, the linear stiffness matrix \mathbf{K}_E of a tensegrity is given as:

$$\mathbf{K}_E = \mathbf{B}\mathbf{D}\mathbf{B}^T \tag{18}$$

which is a symmetric matrix with $3N_V$ rows and $3N_V$ columns. By assuming that the prestress force in member i is F_i , we define a diagonal matrix \mathbf{Q} as:

$$Q_{ii} = \frac{F_i}{L_i} \tag{19}$$

The ratio F_i/L_i is known as the force density. The so-called force density matrix (Zhang and Ohsaki 2015) (or reduced stress matrix; Connelly 1999; Schenk et al. 2007) is then formed by:

$$\mathbf{E} = \mathbf{C}^T\mathbf{Q}\mathbf{C} \tag{20}$$

which is of size $N_V \times N_V$. Then, the geometrical stiffness matrix is constructed by:

$$\mathbf{K}_G = \mathbf{E} \otimes \mathbf{I}_{3 \times 3} \tag{21}$$

where \mathbf{I} is the identity matrix. Finally, the tangent stiffness matrix of a tensegrity is the summation of the linear stiffness matrix and the geometrical stiffness matrix:

$$\mathbf{K} = \mathbf{K}_E + \mathbf{K}_G \tag{22}$$

Appendix 4: Nomenclature

- $\mathbf{1}$ Vector of ones
- \mathbf{B} Equilibrium matrix
- \mathbf{F} Member forces
- \mathbf{G} Incidence matrix
- \mathbf{G}_p Physical contact matrix
- \mathbf{K} Tangent stiffness matrix
- \mathbf{K}_E Linear elastic stiffness matrix
- \mathbf{K}_G Geometrical stiffness matrix
- \mathbf{p} Coordinates of nodes, $3N \times 1$ vector
- \mathbf{s} A binary vector for the presence of struts
- \mathbf{u} Displacement of nodes, a perturbation on \mathbf{p}
- \mathbf{u}_M First-order mechanisms of the dual truss of a tensegrity
- E Edges of a graph
- e An edge (member)
- E_g Edges of the ground structure
- G A graph
- H, K Symmetry groups
- h_i, k_i Symmetry operations
- n, \mathbf{n} Level of discontinuity of struts
- N_I Number of active integer variables

n_r	Number of rigid-body motions
N_{E_g}	Number of members in the ground structure
N_E	Number of members in the obtained tensegrity
N_{V_g}	Number of nodes in the ground structure
N_V	Number of nodes in the obtained tensegrity
T_{opt}	Running time of the optimization
V	Vertices of a graph
v	A vertex (node)
V_g	Vertices of the ground structure
KI	Kinematic indeterminacy

Publisher's note Springer Nature remains neutral with regard to jurisdictional claims in published maps and institutional affiliations.

References

- Bendsøe M, Sigmund O (2003) Topology optimization: theory, methods and applications. Springer
- Calladine CR (1978) Buckminster Fuller's tensegrity structures and Clerk Maxwell's rules for the construction of stiff frames. *Int J Solids Struct* 14:161–172
- Caluwaerts K, Despraz J, İçen A, Sabelhaus AP, Bruce J, Schrauwen B, SunSpiral V (2014) Design and control of compliant tensegrity robots through simulation and hardware validation. *J Royal Soc Interface* 11(98):1–13
- Connelly R (1995) Globally rigid symmetric tensegrities. *Struct Topol* 21:59–78
- Connelly R (1999) Tensegrity structures: why are they stable? In: Thorpe MF, Duxbury PM (eds) Rigidity theory and applications. Kluwer Academic, pp 47–54
- Connelly R, Whiteley W (1996) Second-order rigidity and prestress stability for tensegrity frameworks. *SIAM J Discret Math* 9(3):453–491
- Dorn WS, Gomory RE, Greenberg HJ (1964) Automatic design of optimal structures. *J de Mecanique* 3(1):25–52
- Ehara S, Kanno Y (2010) Topology design of tensegrity structures via mixed integer programming. *Int J Solids Struct* 47(5):571–579
- Felix JJ, Vanderplaats GN (1987) Configuration optimization of trusses subject to strength, displacement and frequency constraints. *J Mechs Trans Autom Des* 109(2):233–241
- Fuller RB (1962) Tensile-integrity structures. United States Patent 3063521
- Godsil C, Royle GF (2001) Algebraic graph theory. Springer, New York
- Guest SD (2000) Tensegrities and rotating rings of tetrahedra: a symmetry viewpoint of structural mechanics. *Philos Trans R Soc London A* 358(1765):229–243
- Guest S (2006) The stiffness of prestressed frameworks: a unifying approach. *Int J Solids Struct* 43(3-4):842–854
- Guest SD (2011) The stiffness of tensegrity structures. *IMA J Appl Math* 76:57–66
- Gurobi Optimization (2014) Gurobi optimizer reference manual. Houston TX: Gurobi Optimization Inc., 6.0 ed
- Hanaor A (2012) Debunking tensegrity - a personal perspective. *Int J Space Struct* 27(2&,3):179–183
- Hanaor BA, Liao M-K (1991) Double-layer tensegrity grids: static load response I: analytical study. *J Struct Eng* 117(6):1660–1674
- Heartney E, Snelson K (2009) Kenneth snelson: forces made visible. Hudson Hills
- Ingber DE (1998) The architecture of life. *Sci Am* 278(1):48–57
- Kanno Y (2012) Topology optimization of tensegrity structures under self-weight loads. *J Oper Res Soc Jpn* 55(2):125–145
- Kanno Y (2013a) Topology optimization of tensegrity structures under compliance constraint. A mixed integer linear programming approach. *Optim Eng* 14(1):61–96
- Kanno Y (2013b) Exploring new tensegrity structures via mixed integer programming. *Struct Multidiscip Optim* 48(1):95–114
- Lee S, Lee J (2016) Advanced automatic grouping for form-finding of tensegrity structures. *Struct Multidiscip Optim* 55(3):959–968
- Li Y, Feng X-Q, Cao Y-P, Gao H (2010a) Constructing tensegrity structures from one-bar elementary cells. *Proc R Soc A* 466(2113):45–61
- Li Y, Feng X-Q, Cao Y-P, Gao H (2010b) A Monte Carlo form-finding method for large scale regular and irregular tensegrity structures. *Int J Solids Struct* 47(14-15):1888–1898
- Liu K, Wu J, Paulino GH, Qi HJ (2017) Programmable deployment of tensegrity structures by stimulus-responsive polymers. *Sci Rep* 7:3511
- Manhattan (2018) Skwish. Image retrieved from: <https://www.manhattantoy.com/collections/skwish/products/skwish-natural>
- Moored KW, Kemp TH, Houle NE, Bart-Smith H (2011) Analytical predictions, optimization, and design of a tensegrity-based artificial pectoral fin. *Int J Solids Struct* 48(22-23):3142–3159
- Motro R (2006) Tensegrity: structural systems for the future. Elsevier
- Ohsaki M, Zhang J (2015) Nonlinear programming approach to form-finding and folding analysis of tensegrity structures using fictitious material properties. *Int J Solids Struct* 69-70:1–10
- Pellegrino S (1992) A class of tensegrity domes. *Int J Space Struct* 7:127–142
- Rimoli JJ, Pal RK (2016) Mechanical response of 3-dimensional tensegrity lattices. *Compos Part B: Eng* 115:30–42
- Rhode-Barbarigos L-G-A (2012) An active deployable tensegrity structure. PhD thesis, École Polytechnique Fédérale de Lausanne
- Schenk M, Guest SD, Herder JL (2007) Zero stiffness tensegrity structures. *Int J Solids Struct* 44(20):6569–6583
- Skelton RE, de Oliveira M (2009) Tensegrity systems. Springer, US
- Smith ODS (1998) Generation of ground structures for 2D and 3D design domains. *Eng Comput* 15(4):462–500
- Snelson K (2012) The art of tensegrity. *Int J Space Struct* 27(2-3):71–80
- Sultan C (1999) Modeling, design, and control of tensegrity structures with applications. PhD thesis, Purdue University
- Taubin G (1994) An accurate algorithm for rasterizing algebraic curves and surfaces. *IEEE Comput Graph Appl* 14:14–23
- Tachi T (2013) Interactive freeform design of tensegrity. In: Hesselgren L, Sharma S, Wallner J, Baldassini N, Bompas P, Raynaud J (eds) Advances in architectural geometry 2012. Springer, Vienna, pp 259–268
- Tibert AG (2002) Deployable tensegrity structures for space applications. PhD thesis, Royal Institute of Technology
- Williamson D, Skelton RE (2003) General class of tensegrity structures: topology and prestress equilibrium analysis. *J Guid Control Dyn* 26(5):685–694
- Xu X, Wang Y, Luo Y, Asce AM (2016) General approach for topology-finding of tensegrity structures. *J Struct Eng* 142(10):04016061
- Zhang JY, Ohsaki M (2015) Tensegrity structures - form, stability, and symmetry. Springer, Japan

- Zhang JY, Ohsaki M (2006) Adaptive force density method for form-finding problem of tensegrity structures. *Int J Solids Struct* 43(18-19):5658–5673
- Zhang L, Maurin B, Motro R (2006) Form-finding of nonregular tensegrity systems. *J Struct Eng* 132(9):1435–1440
- Zhang JY, Guest SD, Ohsaki M (2009) Symmetric prismatic tensegrity structures: part I. Configuration and stability. *Int J Solids Struct* 46(1):1–14
- Zhang X, Ramos AS Jr, Paulino GH (2017) Material nonlinear topology optimization using the ground structure method with a discrete filtering scheme. *Struct Multidiscip Optim* 55:2045–2072
- Zegard T, Paulino GH (2015) GRAND3 - Ground structure based topology optimization for arbitrary 3D domains using MATLAB. *Struct Multidiscip Optim* 52:1161–1184